Mössbauer study of amorphous FeF_3

M. Eibschütz, M. E. Lines, L. G. Van Uitert, H. J. Guggenheim, and G. J. Zydzik
AT&T Bell Laboratories, Murray Hill, New Jersey 07974
(Received 28 November 1983)

An amorphous sample of FeF_3 (enriched in ^{57}Fe) has been prepared by vapor deposition at liquid-nitrogen temperature, and its 4.2-K Mössbauer Zeeman spectrum is reported. The spectrum consists of six well-resolved broad experimental lines, which indicates the existence of a distribution of electric field gradients, hyperfine fields, and isomer shifts at the iron sites. A quantitative analysis of mean line positions, root-mean-square widths, and line shapes of the six Mössbauer lines enables us to obtain new information concerning the statistical distribution of iron environments in the glassy matrix. The electric-field-gradient distribution at the iron sites is composed of equal proportions with positive and negative principal values. The distribution of Zeeman quadrupole-shift energies is very closely of symmetric Gaussian form. The hyperfine-field distribution $p(H)$ possesses a small-amplitude low-field "tail" which at 4.2 K contains $(5\pm2)\%$ of the total sites. A theoretical explanation of the origin and shape of the tail is given, and it is expected to disappear completely in the limit $T\rightarrow0$. The limiting shape of $p(H)$ as $T\rightarrow0$ is quantitatively established and is significantly asymmetric about its peak. Numerical values are given for the separate root-mean-square widths of isomer shift, quadrupole shift, and hyperfine-field distributions and for correlations between these variables.

I. INTRODUCTION

In a series of recent papers[1–4] the Mössbauer quadrupole and Zeeman spectra of ^{57}Fe in an amorphous environment have been analyzed and used specifically to study local structure in vitreous $Y_3Fe_5O_{12}$. This material, whose crystalline form is yttrium iron garnet (YIG), is found to lose all memory of its local crystalline coordination in the amorphous state, and appears to conform with the expectations of a dense random-packed assembly of spheres (of appropriate relative diameters to represent Y^{3+}, Fe^{3+}, and O^{2-}, respectively) modified only to allow for the existence of repulsive Coulomb forces between the trivalent cations.[5]

In the present paper we report the measurement and interpretation of analogous Mössbauer spectra for amorphous FeF_3 (a-FeF_3). This is only the second amorphous insulating material (and first fluoride) for which detailed assessments of Mössbauer parameters, the correlations and variances, etc., have been given. Crystalline FeF_3, like crystalline YIG, is magnetically ordered at room temperature. Unlike crystalline YIG, however, it has only a single resolvable Mössbauer iron site,[6] so that any Mössbauer-parameter correlations (such as those between hyperfine field, isomer shift, quadrupole energy, etc.) which develop in the amorphous phase must necessarily result in their entirety from deformations pertaining to the formation of the noncrystalline state.

Amorphous FeF_3 was first prepared by Ferey *et al.*[7] and found to be paramagnetic down to a temperature $T\approx30$ K, below which a speromagnetic ordering of spins[8,9] develops. Thus, below 30 K the paramagnetic Mössbauer doublet[7,10] (which approximates[10] a direct measure of quadrupole energy distribution at iron sites in the amorphous environment) broadens into a six-line Zeeman spectrum.[11]

In this paper we report on both the preparation of an enriched ^{57}Fe sample of a-FeF_3 and its role in obtaining a Mössbauer Zeeman spectrum at 4.2 K of high statistical quality. A quantitative analysis of mean line positions, root-mean-square (rms) widths, and line shapes of the well-resolved lines enables us to obtain much new information concerning the statistical distribution of iron environments in the glassy matrix. In particular, we obtain the separate rms widths of the distributions of hyperfine field H, isomer shift δ, and first-order Zeeman quadrupole-shift energy u. Additional conclusions include the following.

(1) The electric-field-gradient distribution at iron sites is very accurately composed of equal proportions with positive and negative principal values.

(2) The distribution of Zeeman quadrupole-shift energies is very closely (within 1%) of symmetric Gaussian form.

(3) The hyperfine-field distribution $p(H)$ possesses a small low-field "tail" which, at 4.2 K, contains $(5\pm2)\%$ of the total sites. A theory of the origin of this tail is presented which suggests that it is proportional in amplitude to temperature T, and should therefore disappear completely in the limit $T\rightarrow0$.

(4) The limiting shape of $p(H)$ as $T\rightarrow0$ is significantly asymmetric about its peak [which occurs at $H\approx540$ kOe, a value somewhat smaller than the equivalent crystalline value of 618 kOe (Ref. 6)]. The degree of asymmetry is more than twice the amplitude of its analog in amorphous YIG.[5]

(5) The correlation functions $\mu_N\langle\Delta H\Delta\delta\rangle$ and $\mu_N\langle\Delta H\Delta u\rangle$, involving fluctuations Δx ($x=H,\delta,u$) from their mean values, are, respectively, $+0.031$ and $+0.017$ $(\text{mm/s})^2$. Comparison with the analogous values of $+0.071$ and $+0.028$ $(\text{mm/s})^2$ in a-YIG indicates that the differences are accounted for primarily by the smaller

rms widths of the δ and u distributions in a-FeF_3 (the latter, at least, caused primarily by the lower valence of the anions in the halide material). To the extent that these correlations monitor a characteristic of local disorder, they therefore suggest some common structural features for a-FeF_3 and a-YIG. For a-YIG we believe that a viable model is one based, in lowest order, upon a random packing of spherical ions, subject to a recognition of strong Coulomb forces which maintain a separation between highly ionized cations within the building algorithm.[1–4] For a-FeF_3, on the other hand, the situation is less clear, and an octahedral random-network model[12] is an alternative possibility. As an additional complication, the low-field tail states were not seen[11] in high-field magnetic measurements on a different (unenriched) sample of a-FeF_3. The latter sample was reported[7] to have a low-temperature hyperfine field of (558±1) kOe, considerably larger than in our sample, leaving open the question as to what extent different methods of sample preparation produce amorphous materials with substantially different local environments.

II. EXPERIMENT AND CURVE FITTING

Amorphous ferric fluoride (a-FeF_3) was deposited as film by evaporation of the crystalline material onto graphite, boron nitride, and glass substrates. A sample enriched in ^{57}Fe was deposited only on graphite. A $\frac{3}{4}$-in.-diam graphite substrate was held to a copper block by aluminum-filled epoxy (Epotech), but without adding the hardener so that the samples could easily be removed later. The fluoride was evaporated onto the substrates, and films approximately 50 000 Å thick were obtained in 3 h. The station was first pumped for 24 h to a pressure of 1.2×10^{-6} Torr in order to remove all traces of moisture. Liquid nitrogen was then passed through the block and evaporation initiated. Details on preparation of amorphous FeF_3 have been given elsewhere.[13]

The ^{57}Fe Mössbauer absorption spectra were obtained in a standard transmission geometry using a conventional constant-acceleration spectrometer and a ^{57}Co-in-Pd source. The room-temperature Mössbauer spectra for FeF_3 deposited on boron nitride and glass are identical, within the statistical scatter of the data, to the graphite substrate. The absorber in this experiment was a film of FeF_3 enriched in ^{57}Fe approximately 15 000 Å thick. The room-temperature Mössbauer spectrum[13] of a-FeF_3 has established the existence of a broad quadrupole-doublet distribution with peak-to-peak splitting of 0.55 mm/s and an isomer shift of 0.45 mm/s (with respect to Fe metal at room temperature). The isomer shift indicates that iron in a-FeF_3 is in the Fe^{3+} valence state. We note that our value of 0.45 mm/s for amorphous FeF_3 is slightly smaller than the 0.54-mm/s value reported by Ferey *et al.*[7] for their sample of a-FeF_3. Both values, however, would indicate a ferric state for the constituent iron atoms. The amorphous Mössbauer spectrum is to be contrasted with the single-crystal equivalent.[6] Crystalline FeF_3 has a long-range magnetic order at room temperature, and thereby exhibits a six-line Zeeman-split spectrum. In its paramagnetic phase, crystalline FeF_3 exhibits a single-line spectrum, indicating a zero or negligibly small quadrupole splitting. The spectrum of a-FeF_3 at 4.2 K displays a well-resolved six-line pattern with good statistics and many channels per peak and is given in Fig. 1. The mean hyperfine field is 529 kOe and the mean isomer shift is 0.586 mm/s, again indicating that iron is in the Fe^{3+} valence state.

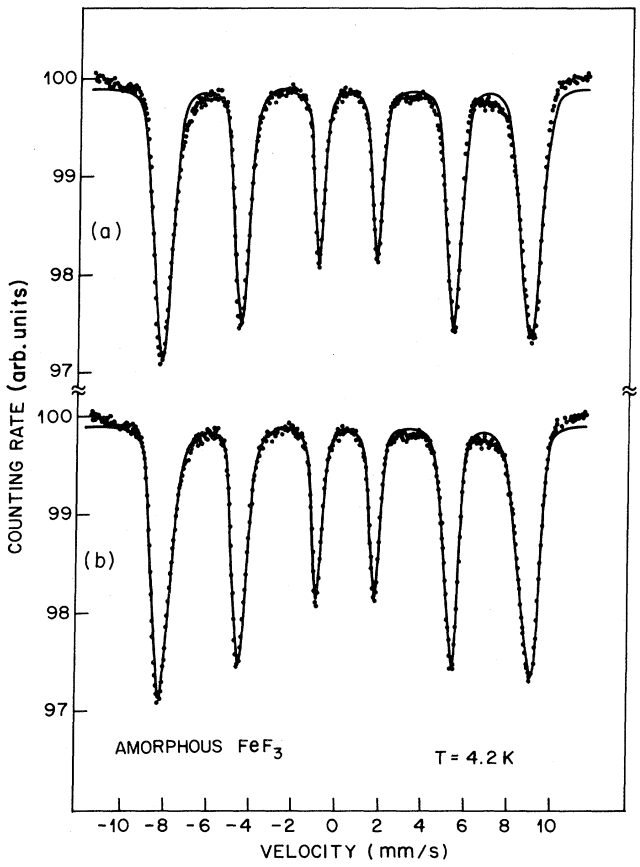

FIG. 1. Experimental ^{57}Fe Mössbauer Zeeman spectrum of a-FeF_3 taken at 4.2 K. The continuous curves are the best nonlinear least-squares fits to the data using six independent (a) symmetric Gaussian and (b) asymmetric Gaussian distributions of natural-width Lorentzian lines. The parameters corresponding to these fits are given in Tables I and II, respectively.

The six broad experimental Zeeman lines (labeled L_1 to L_6 in order of increasing energy) are each composed of a distribution of natural-width Lorentzians. We now represent this Zeeman spectrum as the sum of six such independent distributions $p_i(x)$ in the form

$$f(z)=\sum_{i=1}^{6} h_i \sum_{y=1}^{512} w_L^2 p_i(y-l_1)/[w_L^2+(z-y)^2]\,, \qquad (1)$$

in which y and z are discrete variables running over the 512 channels of the folded experimental data, $w_L=0.10$ mm/s is the Lorentzian half width at half maximum (HWHM), and h_i and l_i are real variables measuring the amplitudes and positions of the six distributions i.

From Fig. 1 we see that the Mössbauer Zeeman spectrum at 4.2 K consists of six well-separated lines so that problems of line deconvolution are minimal. As a first approximation, the independent distributions $p_i(x)$ are ar-

TABLE I. Line positions $l_i=\langle L_i\rangle$, half widths at half heights w_i, and areas A_i of the six symmetric Gaussian distributions p_i of Eqs. (1) and (2) which best fit the Mössbauer Zeeman data of amorphous FeF_3 at 4.2 K; see Fig. 1(a). Line positions are given with respect to the isomer shift $\langle L_1+L_2+L_5+L_6\rangle/4$ as origin.

	i					
	1	2	3	4	5	6
$\langle L_i\rangle$ (mm/s)	−8.6325	−4.9636	−1.3495	1.3606	4.9766	8.6195
$2w_i$ (mm/s)	0.9025	0.6763	0.4323	0.4632	0.6927	1.0163
A_i (arb. units)	1.0175	0.7119	0.3744	0.3853	0.7280	1.0400
$A_1/A_6=0.978$			$A_2/A_5=0.978$			$A_3/A_4=0.972$

bitrarily taken to be of symmetric Gaussian form. Writing

$$p_i(x)=\exp[-x^2(\ln 2)/w_i^2]\,, \tag{2}$$

in which w_i are the respective HWHM's for the individual distributions i, a computer least-squares fit to convergence with the Zeeman data is obtained as shown in Fig. 1(a). This fit provides the "best-fit" parameters given in Table I, where we also include the distribution-area ratios A_1/A_6, A_2/A_5, and A_3/A_4, which should all be unity for the ideal limit of perfect data and fit.

In the symmetric Gaussian approximation the values l_i in Eq. (1) are identically equal to the mean positions of the distributions (which we symbolize as $\langle L_i\rangle$). From Fig. 1(a) it is evident that some degree of asymmetry is present in the individual line shapes (particularly the outside lines), and, in an effort to represent this in the fitting procedure, we have rerun the least-squares computer program, replacing the symmetric Gaussians of Eq. (2) with asymmetric Gaussians of the form

$$p_i^{\pm}(x)=\exp[-x^2(\ln 2)/(w_i^{\pm})^2]\,, \tag{3}$$

in which the $+$ $(-)$ superscript is relevant for $x>0$ $(x<0)$ and the HWHM values w_i^+ and w_i^- are, in general, unequal for each component line i. The best asymmetric Gaussian fit to the data via Eq. (1) is shown in Fig. 1(b), and generates the best-fit parameter values shown in Table II. From them one can calculate the mean values $\langle L_i\rangle$ and variances W_i^2 of the six independent distributions: These values are also quoted in Table II, where we note that $\langle L_i\rangle$ is no longer equal to l_i.

Although, as measured by the minimized least-squares deviation of the model from the data, the asymmetric fit is a factor of 2.83 better than the symmetric equivalent, some obvious discrepancies still remain in the wings of the outside lines. These will be discussed in detail below.

III. ANALYSIS OF LINE POSITIONS

As set out in previous publications[1,2] the mean line positions $\langle L_i\rangle$ can be expressed in terms of five parameters, namely the mean isomer shift $\langle\delta\rangle$, the mean hyperfine field $\langle H\rangle$, and the first- and second-order quadrupole perturbational shifts $\langle u\rangle$ and $\langle\alpha_{\pm}\rangle$. From the symmetric-distribution fit (Table I) we calculate $\langle\delta\rangle=0.591$ mm/s with respect to iron at room temperature, $\langle H\rangle=533.4$ kOe, $\langle\alpha_+\rangle=+0.053$ mm/s, $\langle\alpha_-\rangle=-0.004$ mm/s, and $\langle u\rangle=+0.006$ and -0.007 mm/s, where the two values for the last parameter result from the overdetermination of the problem (six equations and five unknowns).

The computer-determined 70% confidence limits for the mean line position values $\langle L_i\rangle$ are ±0.006 mm/s, leading us to the estimate

$$\langle u\rangle=0.000\pm0.006 \tag{4}$$

for the first-order Zeeman quadrupolar line shift. A value of zero is in accord with theoretical expectations for an amorphous ferric speromagnet (angles θ and ϕ random in Ref. 1), as is the close proportionality $A_6:A_5:A_4:A_3:A_2:A_1\approx3:2:1:1:2:3$ (Table I). However, a

TABLE II. Mean line positions $\langle L_i\rangle$, half widths at half heights w_+ and w_-, areas A_i, and mean-square linewidths $W_i^2=\langle(L_i-\langle L_i\rangle)\rangle^2$ for the six asymmetric Gaussian distributions $p_i^{\pm}$ of natural-width Lorentzian lines which produce the converged least-squares-computed fit to the Mössbauer Zeeman data of amorphous FeF_3 at 4.2 K as shown in Fig. 1(b). Line positions are given with respect to the isomer shift $\langle L_1+L_2+L_5+L_6\rangle/4$ as origin.

	i					
	1	2	3	4	5	6
l_i (mm/s)	−8.8202	−5.0733	−1.3894	1.4026	5.1097	8.8422
$\langle L_i\rangle$ (mm/s)	−8.5669	−4.9263	−1.3338	1.3543	4.9408	8.5524
w_i^- (mm/s)	0.2692	0.2309	0.1773	0.2685	0.4719	0.7304
w_i^+ (mm/s)	0.6429	0.4478	0.2593	0.1974	0.2226	0.3027
A_i (arb. units)	1.0353	0.7197	0.3786	0.3891	0.7365	1.0616
W_i^2 (mm/s)^2	0.1615	0.0869	0.0349	0.0396	0.0921	0.2075
$A_1/A_6=0.975$			$A_2/A_5=0.977$			$A_3/A_4=0.973$

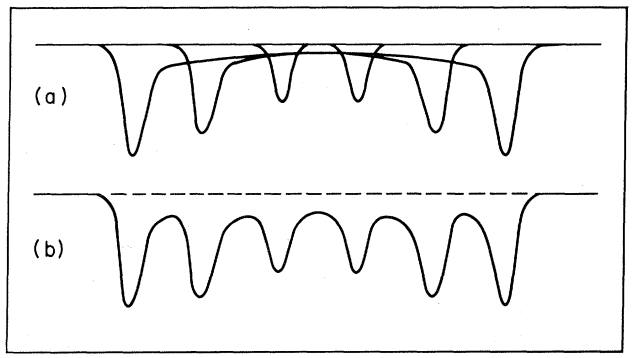

FIG. 2. Schematic iron Mössbauer Zeeman spectrum in an amorphous environment showing (a) the small low-field tails on the resolved field-dominated lines L_1, L_2, L_5, and L_6, and (b) their effect on the resultant (summed) spectrum.

second theoretical expectation for amorphous ferric speromagnet, namely[1] $\langle\alpha_+\rangle=3\langle\alpha_-\rangle$ (which was observed for vitreous YIG), is well outside even the 90% confidence limits in the above analysis.

In order to see whether this last result is connected with the symmetric Gaussian restriction we have repeated the above analysis using the data from Table II appropriate for the improved asymmetric Gaussian fitting procedure. In spite of the almost threefold improvement in fit to the data (as measured by the total mean-square deviation summed over all channels), the discrepancy persists; $\langle\alpha_+\rangle=0.050$ mm/s and $\langle\alpha_-\rangle=-0.005$ mm/s. In fact, the only significant change resulting from the mean-line-position analysis using asymmetric Gaussians is a small decrease (to 529.4 kOe) for the mean hyperfine field.

The origin of the discrepancy lies in a more subtle feature of the line shape, and a clue to its nature can be seen by focusing attention on the significant deviation of the best-fit computer-generated curves in both Figs. 1(a) and 1(b) from the "background" data at the extreme ends of the spectra. An effect of this kind has not appeared in any other of our Gaussian fits to amorphous Zeeman data [e.g., in amorphous YIG (Refs. 1 and 2) or any of the metallic ferromagnetic glasses[14]]. It can be explained by the existence of a long small-amplitude tail on the low-field side of the hyperfine distribution function $p(H)$. This field distribution $p(H)$ completely dominates the outside ($i=1$ and 6) and, to a lesser extent, the middle ($i=2$ and 5) line shapes of the amorphous Zeeman pattern (see Sec. VI), and a tail tends to generate a six-line spectrum of the qualitative form depicted in Fig. 2, which exhibits just the anomaly present in the observed data and which is inexplicable in terms of distributions p_i or $p_i^{\pm}$ of Eqs. (2) and (3). The high-field edge of this tail is clearly shown in the quantitative analysis of the L_1,L_6 line shape set out in Sec. VI.

IV. HYPERFINE TAIL

We propose that the origin of the low-field hyperfine tail arises from the existence of a small fraction of $S=\frac{5}{2}$ ferric spins in the amorphous matrix which experience a resultant *exchange* field $H_{\rm ex}$ (via superexchange interactions with nearest-neighbor spins) for which the energy $g\mu_B H$ (with $g\approx 2$) is not large with respect to kT at $T=4.2$ K. Within the spherical random-packing model of amorphous FeF_3,[15,16] each iron spin $\vec{S}_i$ is coupled magnetically via an exchange energy $-2J_{ij}(\theta_{ij})\vec{S}_i\cdot\vec{S}_j$ to one or more nearest-neighbor spins $\vec{S}_j$ by a dominantly superexchange mechanism via an iron-fluoride-iron ligand path of bond angle θ_{ij}. When $\theta_{ij}\gtrsim 120°$, the superexchange is strongly antiferromagnetic (negative). The magnitude of this exchange decreases with decreasing angle and somewhere in the region $100°<\theta_{ij}<120°$ it goes through zero to become very weakly ferromagnetic close to 90° [see Fig. 3(a)], which is close to the smallest bond angle allowed within the model. We assume that direct iron-iron exchange contributions can be neglected in Fe^{3+} systems.

Via the geometry and packing of the computer-generated assembly of iron and fluorine spheres representing a-FeF_3, it is now possible, using Fig. 3(a), to obtain a qualitative form for the total exchange $\sum_j J_{ij}$, sensed by each iron spin, and therefore to generate the distribution function $p(\sum_j J_{ij})$, within the model. It is sketched in Fig. 3(b). The associated exchange energy distribution

$$p(g\mu_B H_{\rm ex})=p\left[\sum_j 2J_{ij}\vec{S}_j\right]$$

probably mimics $p(\sum_j J_{ij})$ to some extent, although it obviously has a detailed form which depends on the degree and nature of local frustration.[17]

For the present purpose it is necessary only to note that $p(g\mu_B H_{\rm ex})$ has a nonzero probability within the random-packing model as $H_{\rm ex}\to 0$. As a zeroth-order approximation we therefore replace $p(g\mu_B H_{\rm ex})$ by a constant value K for sufficiently small energies. Quite generally, in an exchange field $H_{\rm ex}$ at a temperature T, the equilibrium value of an arbitrary spin is given by

$$\bar{S}=\sum_M M\exp(EM/kT)\Big/\sum_M \exp(EM/kT)\,, \tag{5}$$

where $M=-S,-S+1,\ldots,+S$, and $E=g\mu_B H_{\rm ex}$. This equation shows that $\bar{S}$ does not approach its fully saturated value $\bar{S}=S$ until $E/kT\gg 1$. By formal differentiation of Eq. (5) with respect to E, we obtain

$$\frac{d\bar{S}}{dE}=(1/kT)(\langle S^2\rangle-\langle S\rangle^2)\,, \tag{6}$$

in which the angular brackets represent ensemble averages (i.e., $\langle S\rangle=\bar{S}$). Using this equation we can express the spin distribution function in the form

$$p(\bar{S})=p(E)\frac{dE}{d\bar{S}}=p(E)\frac{kT}{(\langle S^2\rangle-\bar{S}^2)}\,. \tag{7}$$

Since the hyperfine field for orbitally quenched spins is directly proportional to the local spin moment ($H=A\bar{S}$) in the lowest-order contact approximation,[18] and $p(E)=K$ in the "tail region" with $E/kT\lesssim 1$, it follows that we can

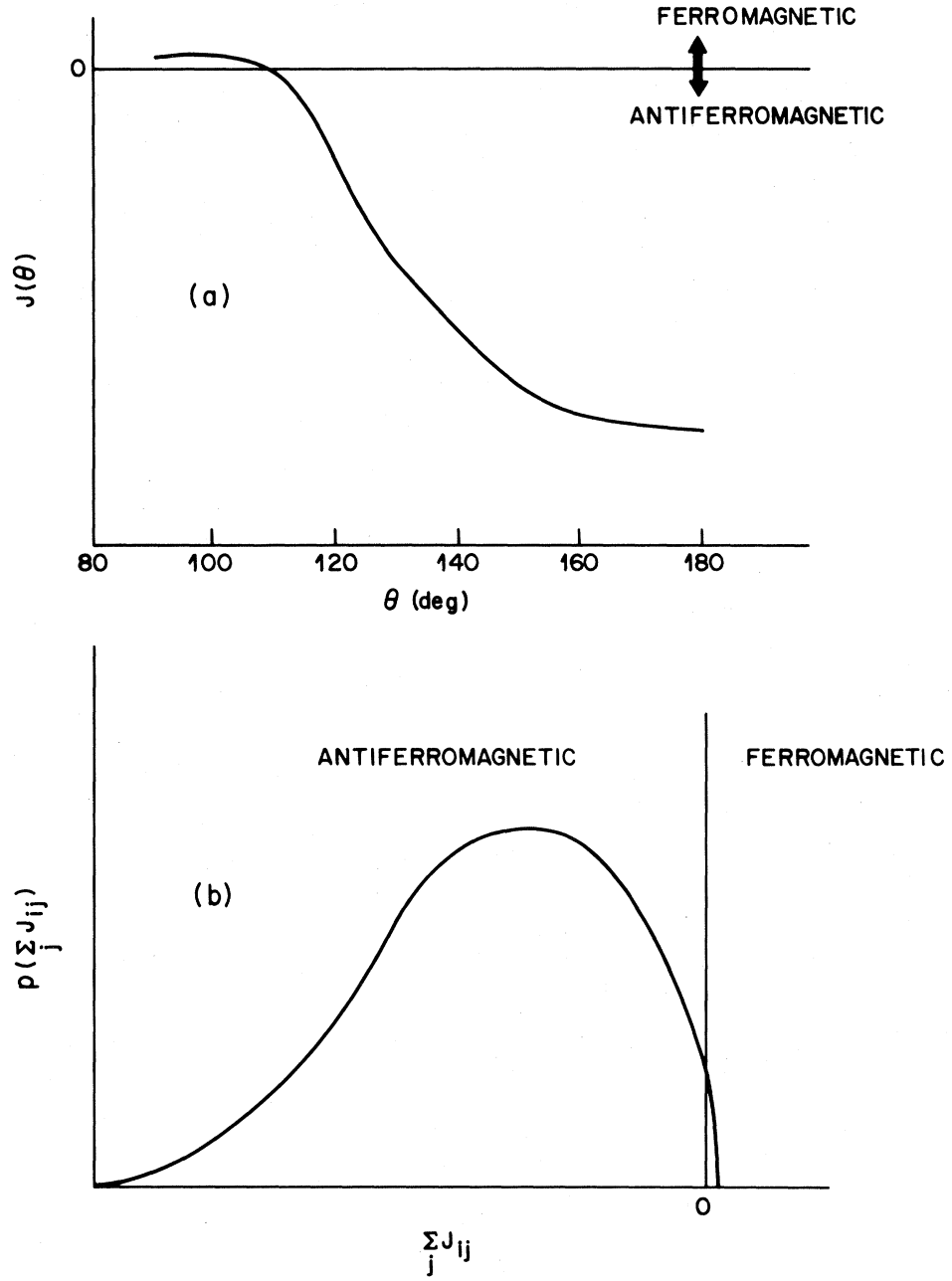

FIG. 3. (a) Exchange energy $J(\theta)$ as a function of the anion bond angle θ in an Fe—F—Fe superexchange configuration. (b) Schematic of the total exchange distribution function $p(\sum_j J_{ij})$ vs total exchange $\sum_j J_{ij}$ in a random-packed computer model of amorphous FeF_3.

express the hyperfine tail in the form

$$p(H)=(K/A)kT/(\langle S^2\rangle-\bar{S}^2)\ . \tag{8}$$

Since $\langle S^2\rangle$ can be directly computed for any spin quantum number via the equation

$$\langle S^2\rangle=\sum_M M^2\exp(EM/kT)\Big/\sum_M \exp(EM/kT)\ , \tag{9}$$

we can, using Eqs. (5) and (9), and eliminating E/kT, calculate $p(H)$ as a function of $\bar{S}/S$, or, equivalently, $H/H_{\max}$, where $H_{\max}=AS$ is the maximum possible value contact hyperfine field. For spin $\frac{5}{2}$, which is that relevant for ferric ions, the function $F=(\langle S^2\rangle-\bar{S}^2)^{-1}$ to which the hyperfine tail is directly proportional, is shown in Fig. 4 as a function of $\bar{S}/S=H/H_{\max}$. At $E/kT=1$, we find values $\bar{S}=1.93$ (77% saturation) and $\langle S^2\rangle=4.57$ (73% saturation). Since the midpoint minimum between Zeeman lines L_1 and L_2 (or equivalently, L_5 and L_6) also corresponds to $\bar{S}/S\approx 0.77$ for the outside Zeeman lines, it is apparent that the condition $E/kT=1$ essentially defines the extent of hyperfine tail in the present context.

For a fixed temperature (e.g., $T=4.2$ K in the present experiments) the hyperfine-field tail can therefore be expressed as

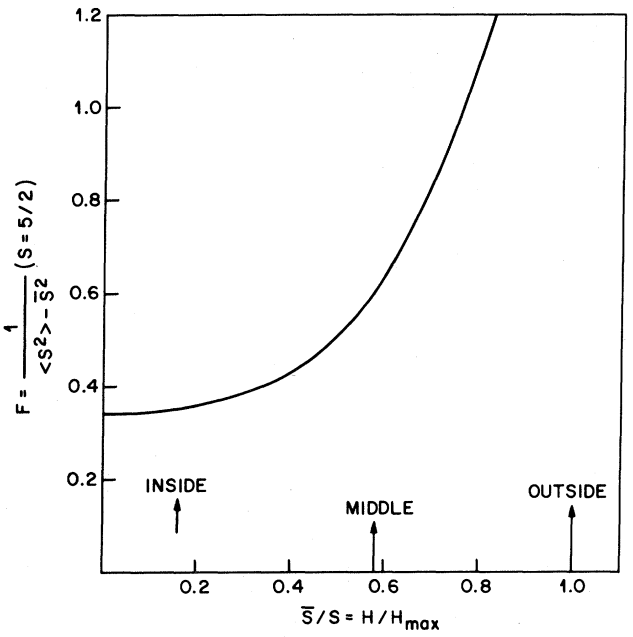

FIG. 4. Function $F=[\langle S^2\rangle-\bar{S}^2]^{-1}$ to which the hyperfine-field tail is directly proportional [Eq. (8)] for $S=\frac{5}{2}$ as a function of $\bar{S}/S=H/H_{\max}$. The arrows indicate the peak positions of inside, middle, and outer lines of the Mössbauer spectrum for an "outside-line" tail.

$$p(H)=BF(H/H_{\max})\,, \tag{10}$$

where B is a constant and the function $F(H/H_{\max})$ is shown in Fig. 4. With the use of this relationship, an approximate estimate of the tail amplitude for a-FeF_3 at 4.2 K can be obtained directly from the experimental data of Figs. 1(a) and 1(b) at the midpoints between L_1 and L_2, and between L_5 and L_6. We find a value $B\approx 0.0016$, which converts to an estimate of $\sim 7\%$ of the total $p(H)$ distribution being in the tail (i.e., with $E\lesssim 4$ K).

From the spherical random-packed computer model of a-FeF_3 we find a value of close to 7% for the percentage of iron sites coordinated to only one or two nearest-neighbor irons via superexchange bonds with bond angles $\theta_{ij}<115°$. Although this close numerical agreement is probably fortuitous, it does suggest, within the model, that the ferromagnetic "potential" exchange[19] via 90° Fe^{3+}–F^-–Fe^{3+} bonds must be very small, i.e., $J(\theta=90°)<1$ K. Unfortunately, we know of no crystalline ferric fluorides with 90° bonds which might lend themselves to testing this hypothesis directly.

In a random-network model of a-FeF_3 the number of $\theta_{ij}<115°$ bonds is negligible, and an explanation of the low-exchange-field sites would have to be sought in the details of local spin frustration. This could arise if some iron sites have nearest-neighbor iron spins whose projections sum to a near-zero value.

In principle, a similar hyperfine tail should also be present in a-YIG. Since it has thus far escaped detection, it must be of much smaller amplitude. This condition might result, we surmise, because 90° Fe^{3+}–O^{2-}–Fe^{3+} band ferromagnetic superexchange is considerably larger than its fluorine equivalent, making $g\mu_B H_{ex}>4$K for most of the topological coordination features which contribute to the tail in the fluorine context. Once again, however, no direct confirmation of this hypothesis is yet available from a study of quasi-90°-bond exchange, e.g., in crystalline ferric oxides such as $CuFeO_2$, (with $\theta_{ij}=96°$). Indeed, the degree to which direct iron-iron exchange interactions might compete with 90° superexchange in these systems also remains unknown.

V. TAIL CORRECTION TO LINE-POSITION ANALYSIS

With the existence of a hyperfine tail on $p(H)$ it is clear that the computer-generated values for $\langle L_i\rangle$, $i=1,2,5,6$ listed in Tables I and II (which are obtained in neglect of the tail) are actually underestimates of the true mean values at 4.2 K. In a simple approximation [assuming all lines $i=1,2,5,6$ are completely dominated in shape by $p(H)$], we can therefore correct the Table I and II values for these particular average line positions $\langle L_i\rangle$, replacing them by values $\lambda\langle L_i\rangle$, and determining the constant λ by *forcing* the condition $\langle\alpha_+\rangle=3\langle\alpha_-\rangle$ (equal to, for instance, 3ϵ) in the line-position analysis of Sec. III. Using the (more accurate) asymmetric analysis from Table II we find values

$$\langle H\rangle=524.0,\quad \langle u\rangle=-0.008\,,$$
$$\epsilon=0.0089,\quad \lambda=0.987\,, \tag{11}$$

with $\langle H\rangle$ given in kOe and $\langle u\rangle$ and ϵ in mm/s. The second-order shift parameter ϵ directly determines the rms pure quadrupole energy distribution $\sigma(E_Q)=\langle(E_Q)^2\rangle^{1/2}$ via the equation[2]

$$\langle(E_Q)^2\rangle=5\,|\,g_E\,|\,\mu_N\langle H\rangle\epsilon\,, \tag{12}$$

in which $g_E=-0.1030$ is the nuclear g factor of the excited Mössbauer level. From Eqs. (11) and (12) we find the Zeeman-estimated quadrupole variance $\langle(E_Q)^2\rangle=0.158$ $(\text{mm/s})^2$ or equivalently $\sigma(E_Q)=0.40$ mm/s. The latter can be compared with direct Mössbauer-doublet estimates in the paramagnetic regime at room temperature[11,13] (0.31 mm/s) and at liquid-nitrogen temperature[20] (0.35 mm/s). The overall agreement (indicating a small increase in quadrupole width with decreasing temperature) supports the viability of the tail-corrected analysis. In particular, it allows us to calculate the variance of u [in $(\text{mm/s})^2$],

$$\langle(\Delta u)^2\rangle=\tfrac{1}{5}\langle(E_Q)^2\rangle=0.032\,, \tag{13}$$

or, equivalently, $\sigma(u)=0.18$ mm/s.

Finally, if the center of "gravity" of the tail states is $H/H_{\max}=x$, then the fraction f of states in the tail is related to λ by the equation

$$1-f+xf=\lambda\,. \tag{14}$$

For a tail shape of the form shown in Fig. 4 we have $x\approx 0.6$ and consequently, from Eq. (14) with $\lambda=0.987$, an estimate $f\approx 3\%$. Both of our independent estimates of tail fraction (7% from Sec. IV and 3% here) are dependent on a knowledge of tail shape. The discrepancy, which we may incorporate within the error bars,

TABLE III. Summary of the findings of the present paper for the mean values $\langle x \rangle$, rms fluctuations $\sigma(x)$, and correlations $\langle \Delta x \Delta y \rangle$ for $x,y = H$ (hyperfine field), δ (isomer shift), and u (first-order quadrupolar Zeeman line shift) as $T \to 0$ in amorphous FeF_3.

$\langle u \rangle = -0.008$ mm/s
$\langle H \rangle = 529$ kOe (peak value at 540 kOe)
$\langle \delta \rangle = 0.586$ mm/s (with respect to iron metal at room temperature)
$\sigma(u) = 0.18$ mm/s
$\sigma(H) = 24.1$ kOe
$\sigma(\delta) = 0.08 \pm 0.02$ mm/s
$\mu_N \langle \Delta H \Delta \delta \rangle = +0.031$ (mm/s)^2
$\mu_N \langle \Delta H \Delta u \rangle = +0.017$ (mm/s)^2

$$f = 0.05 \pm 0.02 , \tag{15}$$

may indicate a deviation from the "constant–density-of-states" approximation of Fig. 4 or may simply result from the smallness of the effect combined with the statistical accuracy of the data and analysis.

VI. LINEWIDTHS AND LINE SHAPES

Assuming that the states in the hyperfine tail at 4.2 K are not grossly atypical in terms of their saturation field in the limit $T \to 0$, the linewidth values in Table II should be representative of the fully saturated $\bar{S} \to S$ spin system. They may therefore be analyzed in conventional fashion as set out in Ref. 1. Using the rms widths W_i^2 directly from Table II in the linewidth 'difference equations' [Eqs. (12) of Ref. 1], we find field correlations [given in (mm/s)^2]

$$\mu_N \langle \Delta H \Delta \delta \rangle = +0.031, \quad \mu_N \langle \Delta H \Delta u \rangle = +0.017 , \tag{16}$$

where $\Delta x = x - \langle x \rangle$ ($x = H, u, \ldots$, etc.). Correlations $\langle \Delta \delta \Delta \alpha_{\pm} \rangle$ are too small [< 0.001 (mm/s)^2] to be reliably estimated.

From the overdetermined lowest order linewidth "sum equations," viz.,

$$\tfrac{1}{2}(W_1^2 + W_6^2) = a^2 + g_1^2 b^2 , \tag{17a}$$

$$\tfrac{1}{2}(W_2^2 + W_5^2) = a^2 + g_2^2 b^2 , \tag{17b}$$

$$\tfrac{1}{2}(W_3^2 + W_4^2) = a^2 + g_3^2 b^2 , \tag{17c}$$

in which $g_1 = 0.2448$, $g_2 = 0.1418$, and $g_3 = 0.0388$,

$$a^2 = \langle (\Delta \delta)^2 \rangle + \langle (\Delta u)^2 \rangle, \quad b^2 = \mu_N^2 \langle (\Delta H)^2 \rangle , \tag{18}$$

we find the solution with smallest rms deviation to be $a^2 = 0.036$ and $b^2 = 2.50$ (mm/s)^2, leading to the standard deviations

$$\begin{aligned} &\sigma(\delta) = 0.06 \to 0.10 \text{ mm/s} , \\ &\sigma(H) = 24.1 \text{ kOe } (1.58 \text{ mm/s}) , \end{aligned} \tag{19}$$

the spread in values for $\sigma(\delta)$ depending on whether one takes the second-order Zeeman [0.032 (mm/s)^2] or pure-quadrupole liquid-nitrogen [0.025 (mm/s)^2] values as being the more accurate representation for $\langle (\Delta u)^2 \rangle$ as $T \to 0$. The deviations of the right-hand side of Eqs. (17) using $a^2 = 0.036$ and $b^2 = 2.50$ from the experimentally determined left-hand side, are, respectively, -0.0011, $+0.0034$, and -0.0023 (mm/s)^2 for Eqs. (17a), (17b), and (17c).[15] These numbers reflect the smallness of the correlations of the type $\langle \Delta \delta \Delta u \rangle$ and $\langle \Delta H \Delta \alpha_{\pm} \rangle$ which have been omitted from Eqs. (17).

Our final findings for mean values, correlations, and distribution widths for the Mössbauer parameters of *a*-FeF_3 as $T \to 0$ are set out in Table III. We note, in particular, the contributions $g_j^2 \langle (\Delta H)^2 \rangle$, $\langle (\Delta u)^2 \rangle$, and $\langle (\Delta \delta)^2 \rangle$ of hyperfine-field, quadrupole-, and isomer-shift distributions to mean-square linewidths for the outer, middle, and inner ($j = 1,2,3$) Zeeman lines: They are

	Hyperfine	Quadrupole	Isomer
Outer: L_1, L_6	0.150	0.032	0.007(3)
Middle: L_2, L_5	0.050	0.032	0.007(3)
Inner: L_3, L_4	0.004	0.032	0.007(3)

(20)

in units of (mm/s)^2. Thus the inner lines are dominated by quadrupole distribution and the middle and outer lines by hyperfine-field distribution. However, for the middle lines, L_2 and L_5, the field dominance is not overwhelming, and our earlier approximation (Sec. V) that the middle line shapes, like the outer ones, reflect the hyperfine distribution alone, is evidently not quantitatively correct.

On the other hand, the very marked dominance of inner linewidth by quadrupole broadening allows us to analyze the L_3 and L_4 line shapes in order to determine the distribution $p_u(E)$ of quadrupole shifts quite accurately. In Fig. 5 we show the computer-generated residuals $R_3(E)$ and $R_4(E)$ from the best *symmetric* Gaussian fit of Fig. 1(a) for lines L_3 and L_4. As explained in Ref. 3, the function $\frac{1}{2}[R_3(E) + R_4(E)]$, which is shown in Fig. 5(c), measures the deviation of $p_u(-E)$ from a symmetric Gaussian form. This deviation, from Fig. 5(c), is found to be extremely small (less than 1% of the distribution amplitude) and is exactly symmetric about the distribution center (defined as $E = 0$). This symmetry establishes[3] that the number of iron sites with positive and negative electric field gradient (EFG) in *a*-FeF_3 is very accurately equal. Finally the degree of asymmetry about the line centers seen [Figs. 5(a) and 5(b)] in $R_3(E)$ and $R_4(E)$ separately (approximately $\pm 2.5\%$ of total line amplitude) reflects the small field-dependent contribution to inner line shape and the asymmetry of the hyperfine-field distribution function

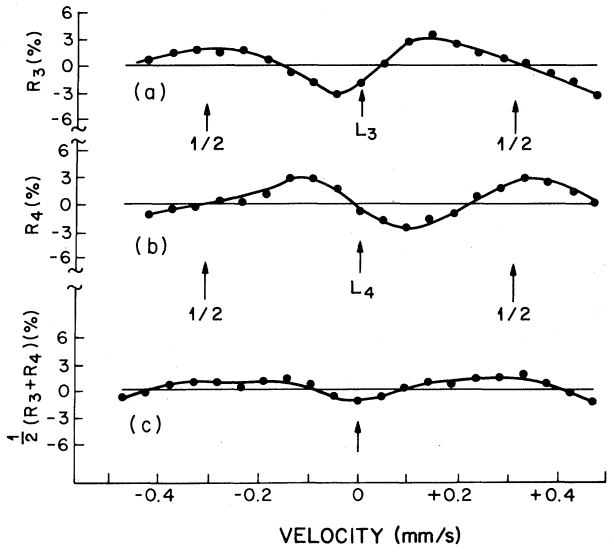

FIG. 5. (a) and (b) show the residuals R_3 and R_4 for the two inner Mössbauer Zeeman lines L_3 and L_4 measuring the difference between the data points and the best-fit-computer-generated symmetric Gaussian curve of Fig. 1(a) scaled as a percentage of peak height. The continuous curves are merely guides to the eye. The arrows labeled L_3 and L_4 denote the peaks of the two Zeeman lines and those labeled $\frac{1}{2}$ the widths at half height. The velocity scale for each line is zeroed at the peak value. (c) The non-Gaussian component of the distribution of first-order Zeeman quadrupole shifts calculated by averaging the L_3 and L_4 residuals of (a) and (b) (see text and Ref. 3). Its lack of asymmetry about its center establishes that the number of iron sites with positive and negative EFG's is very accurately equal in a-FeF_3.

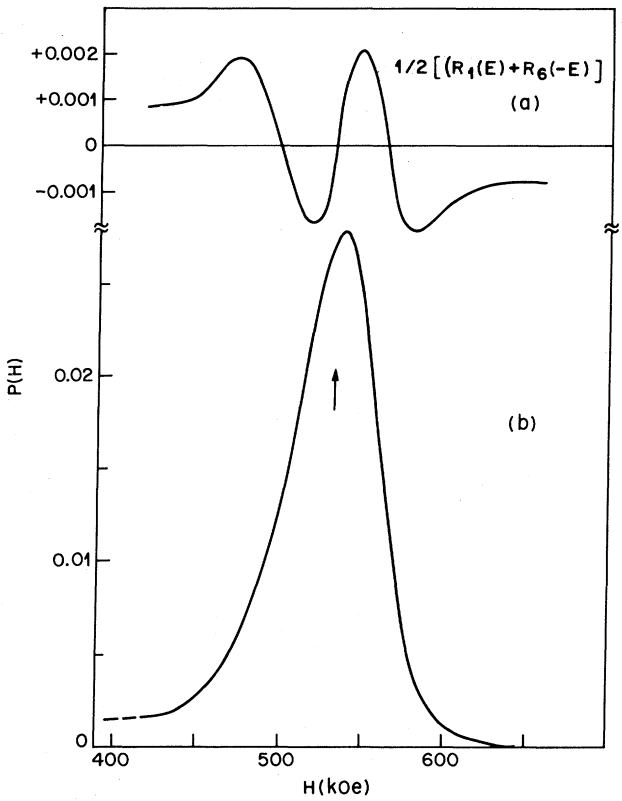

FIG. 6. (a) Asymmetric component of hyperfine-field-generated line shape calculated by averaging the L_6 and energy-reversed L_1 residuals of Fig. 1(a) for a-FeF_3 at 4.2 K. (b) The unnormalized total hyperfine-field distribution line shape $p(H)$ obtained by adding curve (a) to the average symmetric Gaussian best fit to lines L_1 and L_6. Velocity units have been converted to magnetic field units in the abscissa.

$p(H)$. The close equality in number of iron sites with positive and negative EFG's is expected within the random-packing model of a-FeF_3, and also, presumably (since crystalline FeF_3 has an unmeasurably small EFG itself[6]), within any distorted network model as well.

Details of the asymmetry of field distribution $p(H)$ can accurately be computed from the shapes of the lines $i=1$ and 6 which are overwhelmingly dominated by field distribution. In such a situation[5] the hyperfine-field energy distribution $p_H(E)$, which is directly proportional to $p(H)$, has an asymmetric part which is measured by the function $\frac{1}{2}[R_6(E)+R_1(-E)]$. This function, involving the residuals R to lines L_1 and L_6 as generated by the symmetric Gaussian fit of Fig. 1(a), is shown in Fig. 6(a). The detailed form of the complete distribution $p_H(E)$ is then found by adding this asymmetry function to the average symmetric Gaussian best fit to the outside Zeeman lines. The result, plotted in Fig. 6(b), is expressed in field units and therefore represents an unnormalized measure of $p(H)$.[21]

The degree of asymmetry, as measured by the ratio of the amplitudes of Figs. 6(a) and 6(b), is about 7%, which may be compared with a value of 3% for the analogous degree of asymmetry in a-YIG.[5] Finally, we note that the high-field edge of the low-field tail of $p(H)$ is clearly visible in Fig. 6(b). It cannot be reliably extended to lower-field values by this method because of the developing line overlaps with L_2 and L_5.

[1]M. Eibschütz and M. E. Lines, Phys. Rev. B 26, 2288 (1982).
[2]M. Eibschütz and M. E. Lines, Phys. Rev. B 25, 4256 (1982).
[3]M. E. Lines and M. Eibschütz, Phys. Rev. B 25, 6042 (1982).
[4]M. Eibschütz, M. E. Lines, and K. Nassau, Phys. Rev. B 21, 3767 (1980).
[5]M. E. Lines, Phys. Rev. B 20, 3729 (1979); in *Essays in Theoretical Physics,* edited by W. E. Parry (Pergamon, Oxford, 1984).
[6]G. K. Wertheim, H. J. Guggenheim, and D. M. E. Buchanan, Phys. Rev. 169, 465 (1968); Phys. Rev. B 2, 1392 (1970).
[7]G. Ferey, A. M. LeClerc, R. de Pape, J. P. Mariot, and F. Varret, Solid State Commun. 29, 477 (1979).
[8]J. M. D. Coey, J. Appl. Phys. 49, 1646 (1978).
[9]U. Krey, J. Magn. Magn. Mater. 6, 27 (1977).
[10]M. E. Lines and M. Eibschütz, Phys. Rev. B 27, 5308 (1983).
[11]G. Ferey, F. Varret, and J. M. D. Coey, J. Phys. C 12, L531 (1979).

[12]J. M. D. Coey and P. J. K. Murphy, J. Non-Cryst. Solids 50, 125 (1982).
[13]M. Eibschütz, M. E. Lines, L. G. Van Uitert, H. J. Guggenheim, and G. J. Zydzik, Phys. Rev. B 24, 2343 (1981).
[14]M. Eibschütz, M. E. Lines, and H. S. Chen, Phys. Rev. B 28, 425 (1983); J. Phys. F 14, 505 (1984).
[15]M. E. Lines, Phys. Rev. B 21, 5793 (1980).
[16]M. E. Lines, J. Non-Cryst. Solids 46, 1 (1981).
[17]G. Toulouse, Commun. Phys. 2, 115 (1977).
[18]A. Abragam, *The Principles of Nuclear Magnetism* (Clarendom, Oxford, 1961).
[19]P. W. Anderson, in *Solid State Physics,* edited by F. Seitz (Academic, New York, 1963), Vol. 14, p. 99.
[20]M. Eibschütz, unpublished data.
[21]Although accurate in shape, $p(H)$ of Fig. 6(b) still contains small isomer-shift and quadrupole contributions to width. These, from Eq. (20), can be eliminated by reducing the scale of the abscissa about the line peak by $\approx 11\%$.